Optimal Pacing Sites in Cardiac Resynchronization by Left Ventricular Activation Front Analysis

Short Title: LV activation front and CRT

Mohammad Albatat[1,2*], Hermenegild Arevalo[3], Jacob Bergsland[1], Vilde Strøm[3], Ilangko Balasingham[1,4], Hans Henrik Odland[5]

[1] Intervention Centre, Oslo University Hospital, Oslo, Norway

[2] Institute of Clinical Medicine, University of Oslo, Oslo, Norway

[3] Department of Computational Physiology, Simula Research Laboratory, Fornebu, Norway

[4] Department of Electronic Systems, Norwegian University of Science and Technology, Trondheim, Norway

[5] Department of Cardiology, Oslo University Hospital, Oslo, Norway

* Corresponding author

Email: malbatat.90@gmail.com

Adresse:

Oslo University Hospital, Rikshospitalet
Intervention Center
POB 4950 Nydalen
0424 Oslo
Norway

Mob.: +47 4621 2075
Tlf.: +47 2307 0160
Fax: +47 2307 0110

Abstract

Cardiac resynchronization therapy (CRT) can substantially improve dyssynchronous heart failure and reduce mortality. However, about one-third of patients who are implanted, derive no measurable benefit from CRT. Non-response may partly be due to suboptimal activation of the left ventricle (LV) caused by electrophysiological heterogeneities. The goal of this study is to investigate the performance of a newly developed method used to analyze electrical wavefront propagation in a heart model including myocardial scar and compare this to clinical benchmark studies. We used computational models to measure the maximum activation front (MAF) in the LV during different pacing scenarios. Different heart geometries and scars were created based on cardiac MR images of three patients. The right ventricle (RV) was paced from the apex and the LV was paced from 12 different sites, single site, dual-site and triple site. Our results showed that for single LV site pacing, the pacing site with the largest MAF corresponded with the latest activated regions of the LV demonstrated during RV pacing, which also agrees with previous markers used for predicting optimal single-site pacing location. We then demonstrated the utility of MAF in predicting optimal electrode placements in more complex scenarios including scar and multi-site LV pacing. This study demonstrates the potential value of computational simulations in understanding and planning CRT.

1 Introduction

Heart failure (HF) is a major health and socio-economic problem affecting more than 26 million people globally. Prevalence is increasing as the population is getting older [1]. About one-third of HF patients have disorders of the cardiac conduction system causing dyssynchronous ventricular contraction and relaxation patterns, characterized by prolonged QRS duration seen on 12-lead ECG [2]. Cardiac Resynchronization Therapy (CRT) may improve pumping mechanism and HF symptoms for such patients [3, 4], however about 30 % of patients selected according to international guidelines do not respond to CRT [4, 5]. In a subset of patients, non-response can be explained by suboptimal activation of the left ventricle (LV) [6]. Strategies for selection of pacing sites using preoperative or acute clinical parameters have been disappointing [7]and multicentre trials have not provided specific or sensitive response-related acute factors predicting results from CRT [8], nor provided evidence of an optimal pacing configuration[8, 9]. This leaves us with the paradox that to benefit the majority of patients with an indication for CRT, a minority will experience adverse outcomes [10].

Advances in computational modeling of heart-function have made it possible to evaluate different aspects of CRT in a controlled, analytical setting [11], such as evaluating optimal single-site pacing (SSP) from the LV related to scar location [12, 13] and scar size [14]. Other studies focused on creating patient-specific models to aid CRT implementation [15]. The lack of a standard method for the prediction of CRT outcomes has led to a variety of computational studies that have used various intra-procedural, electrophysiological measurements to alleviate this problem. Pressure gradients dP/dt_{max} [15], electromechanical activation sequences [16], ATP consumption heterogeneity [17], and LV endocardium activation times [18] have been used without consistent success.

In this study, we investigated the electrical activation propagation throughout the ventricles and introduce the term *maximum activation front* (MAF) as a potential outcome measurement in a detailed electrophysiological model of infarcted left ventricles. The main objective of the study was to evaluate this novel parameter and to compare it with standard observations used for CRT therapy. Current clinical evidence implies that the optimal LV pacing site is in the latest, spontaneously activated area [2, 9]. We hypothesized that pacing in these areas would produce the highest MAF values. Our secondary objective was to test how building a model for theoretical optimal resynchronization by pacing from multiple nodes could become a benchmark for testing in clinical multisite CRT- pacing.

In section 2, the computational model framework and the study design are described, followed by results in section 3. Finally, the results are discussed, and conclusions are drawn in section 4.

2 Methods

2.1 Geometric data

The geometric models used in this study were generated using contrast-enhanced cardiac MRI to reconstruct patient-specific 3D meshes of the ventricles. A detailed description of the model creation can be found in [19] and is summarized here. Ventricular MRI slices were semi-automatically segmented into four areas, separating LV and RV endo- and epicardium, using Segment™ (Medviso, Sweden). Infarcted regions – appearing white in the contrast-enhanced MRI images – were segmented in each slice. To compensate for movement artifacts during MRI acquisition, segmented areas were aligned using MATLAB Medical Image Processing Toolbox™ (The MathWorks Inc., USA). Post-adjusted data were extracted and converted into five separate surfaces (LV and RV endocardium, LV and biventricular epicardium, and infarct). Surface meshes were created using Visualization Toolkit (VTK) [20], an open-source software system for 3D computer graphics and image processing. A coherent 3D finite element tetrahedral mesh was created based on the separate surfaces using Gmsh [21]. Each resulting mesh comprised of ~2 million nodes and ~10 million elements. Rule-based fiber orientations were assigned to the acquired 3D mesh based on a set of histologically validated myocardial fiber properties [22]. The image-based model creation pipeline is shown in Fig 1.

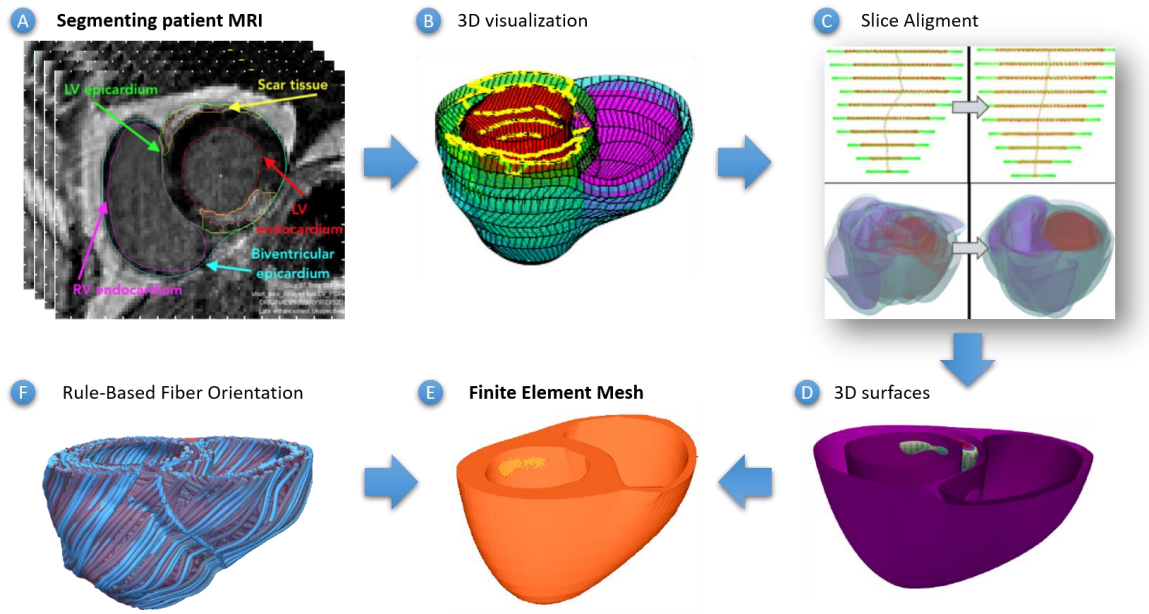

Figure 1 Creation of finite element mesh from patient MRI. A) Each slice between the base and the apex of the cardiac MRI divided into relevant areas. B) The resulting segmentation visualized in Segment™. C) Illustration of movement artifact correction in the first row, spatial alignment in the second row. D) Vizualizing the resulting 3D surfaces. E) The resulting Finite Element Mesh created using Gmesh. F) Rule-based fiber orientation assigned.

The patient MRIs were acquired in the study by Jabbari et al [23]. Patient 1 had a posterolateral infarct involving ~25 % of LV-volume, Patient 2 had a posteroseptal infarct ~15 % of LV, and Patient 3 had an anterior infarct ~10 % of volume (Fig. 2). The LV wall volumes of the three patients were 128.46 cm^3, 123.95 cm^3, and 117.45 cm^3 respectively. To separate the grey-zones (GZ) from the infarct scar, the elements of the ischemic region were subdivided into uniformly spaced onion-like layers toward

the center of the infarct. The outer 20 % of layers were assigned to be GZ and the remaining layers to scar. To simulate various scar sizes in Patient 1, the outer layers were assigned to be non-infarcted and the GZ moved inward to account for 20 % of the remaining infarct layers. Three additional scenarios were made with infarct volumes of 10 %, 5 %, 1.5 % of the ventricular volume. Control scenarios with no infarct were also created. (Fig. 2).

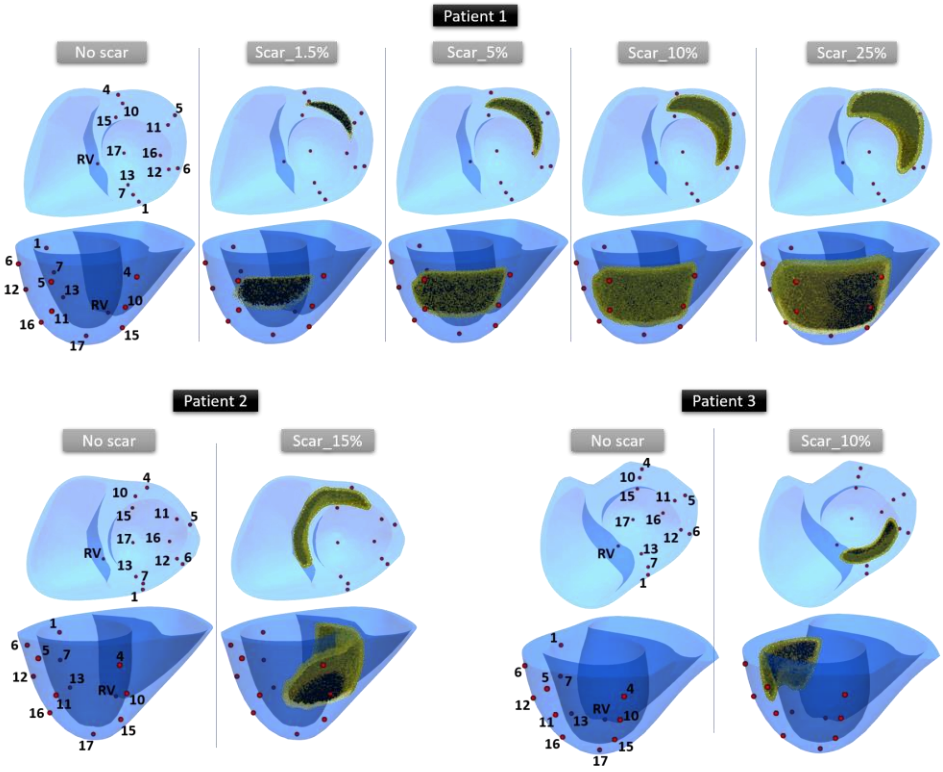

Figure 2 Ventricular geometries and pacing sites. The images on top are the short-axis view and the bottom ones are long-axis views. The RV site is placed in the RV apex endocardium. The 12 LV sites are placed in the center of each LV segment, excluding the septal segments.

2.2 Electrophysiological model

Electrical propagation in the myocardium was modeled using monodomain approximation. The electrophysiological (EP) properties of the three regions – scar, GZ, and healthy – were described as follows: The healthy elements were assigned human ventricular action potential dynamics using the model of Ten Tusscher et al. [(24)] with cell-to-cell conductivities of 0.255 and 0.0775 Sm-1 in the longitudinal and transverse directions, respectively [(25, 26)]. Scar elements were considered electrically non-conductive. EP dynamics of GZ were modeled by adjusting the ionic model of healthy regions based on experimentally validated recordings [(27-29)]. The conductivity of GZ was reduced by 90 % in the transverse direction [(30)]. The software package CARPentry (available at https://carp.medunigraz.at/carputils/), implemented in the Abel Cluster (http://www.hpc.uio.no) was used to perform the simulations. This software has been previously validated and optimized to simulate the electrical behavior of human hearts with high accuracy and efficiency [(31, 32)]. A sample input file (.par file) is provided in Supplement 1.

2.3 Stimulation protocol

To facilitate the analysis, LVs were segmented into 17 segments, defined according to AHA-zone representation [33]. Twelve epicardial pacing sites were located at the center of each of the 12 non-septal segments. Segments located in the septum (2, 3, 8, 9, and 14) were not paced since the LV is not paced from the septum in CRT, but stimulated by the RV site. The 12 pacing sites with their acronyms are listed in Table 1. The RV was stimulated endocardially from the RV apex, like in typical CRT. In addition to the RV-site, the LV was stimulated from 12 LV individual sites (SSP) and two sites simultaneously (Dual site pacing (DSP)). For dual-site stimulations, all possible combinations of site pairs were simulated, resulting in 66 different configurations. For the 25% scar scenario in Patient 1, stimulation from 3 LV sites (TSP) was also investigated. TSP was limited to this one model to reduce computational time. The resulting stimulation configurations for each heart scenario are:

1) RV-only (1 simulation)
2) RV + 1 LV (12 simulations)
3) RV + 2 LV (66 simulations)
4) RV + 3 LV (220 simulations, performed only in Patient 1, scar 25%)

2.4 Maximum Activation Front (MAF) calculation

The simulations' output was the recorded time when each node had been activated. To analyze the activation front propagation, the activated elements were recorded in a moving window of 10 ms. This means that the volume at each time point represents the activated volume from 5 ms before to 5 ms after that time point. Supplementary Video 1 shows an example of the activation front propagation from Patient 1 with no scar pacing only from the RV site. Fig. 3 shows the volume of activated LV elements plotted against time. The recruited volumes are divided by the total LV volume to normalize the results. The recruited volume ratio is used for presenting the results. Different moving window sizes could have been used, but 10 ms was selected since graphs became smoother without distortion of results.

To understand the morphology of the activation front, the outcome of RV-only pacing (baseline) is compared to the outcome of pacing all endocardial (all_endo) mesh elements except the basal ones (upper third of the ventricles) simultaneously, which is considered the best-case scenario since it mimics Purkinje activation. As seen in Fig. 3, the recruitment curves have four main features that describe the LV activation pattern:

1) Upstroke. Describing the initial magnitude of the activation front.
2) The peak. Representing the maximum volume of the activation front (MAF).
3) The area under the graph, which is the total volume of the LV myocardium.
4) The end of the graph, depicting the time it took to activate the whole ventricle, the so-called total activation time (TAT).

The goal of CRT is to generate LV recruitment curves as close as possible to the best-case scenario shown in Fig. 3, represented by the yellow curve. Steeper upstroke leads to higher pressure build-up indicating faster *recruitment* of myocytes, while shorter TAT indicates narrower QRS complex in an ECG. Since the area under the graph is constant in all pacing scenarios, higher MAF means more LV volume is recruited within a short period, which can be achieved by either shortening TAT, making the upstroke steeper, or both. Thus, higher MAF indicates more synchronous LV activation and is used here as the outcome measure.

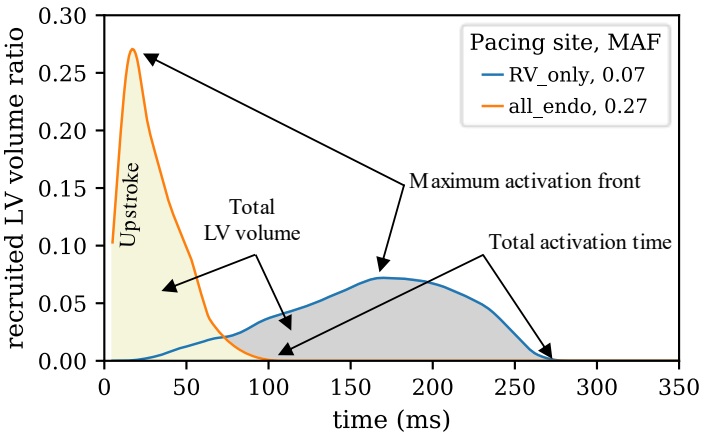

Figure 3 LV activation front graphs of baseline pacing and pacing all endocardial nodes simultaneously.

3 Results

3.1 Single-Site Pacing (SSP)

To evaluate the propagation delay between the RV site and the different LV sites, we recorded the activation time at the 12 LV sites when pacing from only the RV-site i.e. the time it takes the stimulus from the RV-site to reach the different LV sites. Table 1 shows the different timings for all 3 patients with no scar. Note that the posterior sites have the longest activation delay, while the apical sites have the shortest, due to 1) the RV site is closer to the apical sites; 2) the posterior sections of the LV in the included patients are thicker and the stimulus propagates through more tissue.

LV Site	Location		Acronym	Activation time (ms)		
				Patient 1	Patient 2	Patient 3
1	Basal	Anterior	bas.a	157.3	142.3	168.3
4		Posterior	bas.p	229.5	257.4	200.2
5		Posterolateral	bas.p-l	246.3	240.7	232.3
6		Anterolateral	bas.a-l	217.2	200.3	250.4
7	Mid	Anterior	mid.a	124.1	134.1	144
10		Posterior	mid.p	180.3	212.2	164
11		Posterolateral	mid.p-l	220.6	225.7	179.1
12		Anterolateral	mid.a-l	196.2	195.9	207.8
13	Apical	Anterior	api.a	109.9	114.7	80.7
15		Posterior	api.p	137.1	151	129.5
16		Lateral	api.l	189.2	194.1	127.3
17		Apex	apex	83.5	96.5	68.1

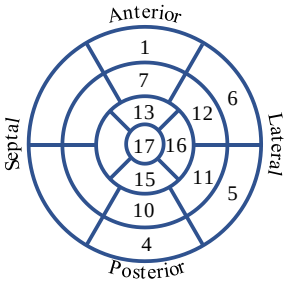

Table 1 LV pacing sites locations, acronyms and activation delay, which is the time it takes the RV stimulus to reach the different sites. Note that the pacing site locations are used to record the time the RV-site stimuli activate them. The illustration on the right-hand side shows the location of the different sites in the Bull's eye representation of the LV.

To understand the effect of changing pacing site location, the recruitment curves of the various pacing configurations in Patient 1 without a scar and with the largest scar are analyzed first.

The results of the 12 SSP sites are divided into three categories based on the location of the pacing electrode: apical sites, anterior sites, and posterior sites. As shown in Fig. 4 A, in the no-scar scenario, all pacing sites improve upstroke and TAT compared to baseline (RV-only pacing). While the apical and anterior sites only slightly changed MAF, the posterior sites produced higher MAF values. It appears that pacing from the sites with the longest activation delay (see Table 1) produces the highest MAF, the overall correlation between activation delay and MAF is not conclusive with r = 0.658, n = 12, p = 0.02. The lowest MAF was produced by bas.a site, 5 % *lower* than the baseline. The graph (orange line in Fig. 4) has a sharp upstroke with a flat peak, which indicates that a larger section of the LV is activated faster than the rest, relatively increasing activation desynchrony. The mid.p-l site produced the highest MAF, 40 % *higher* than the baseline. Video 2 shows a sequence of MAF produced by the best and worst pacing configurations. It clearly shows that the MAF of Worst SSP (bas.a) pacing had only one activation front since it merged with the activation front of the RV-site early. In Best SSP (mid.p-l) however, both activation fronts are separated, and MAF is achieved once they start merging at a later stage.

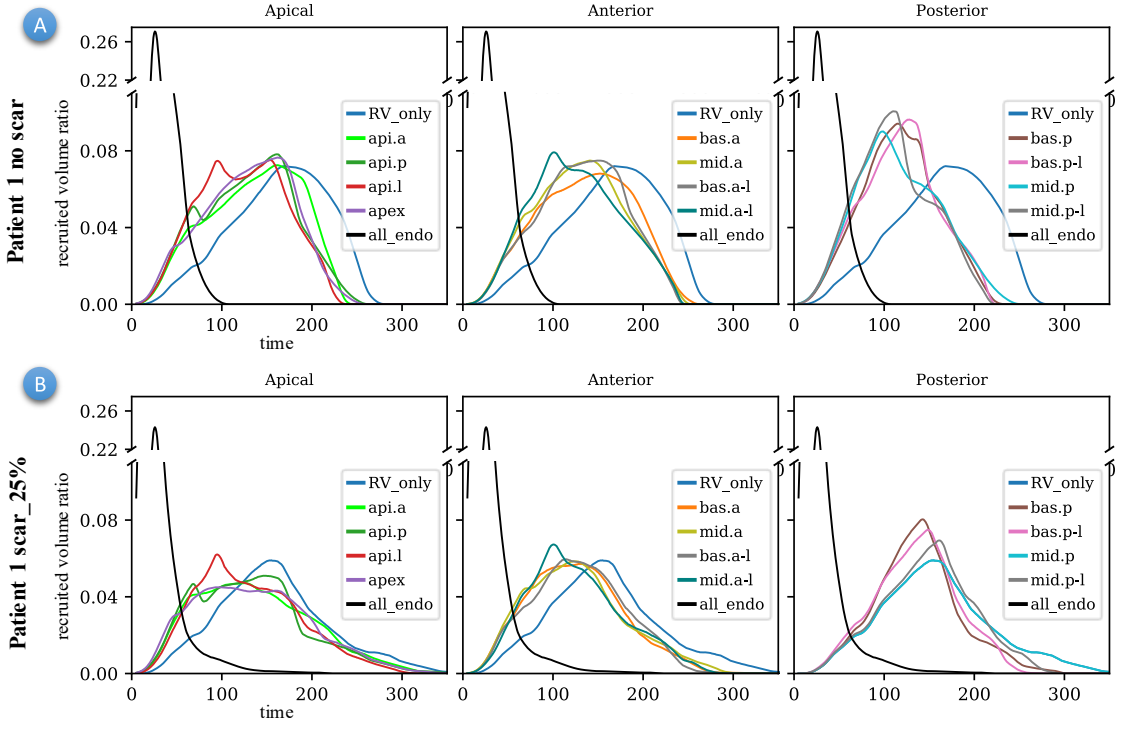

Figure 4 LV activation front graphs when pacing from the different pacing sites, divided into apical, anterior and posterior regions. A: The results of Patient 1 without scar. B: The results of Patient 1 with scar_25%.

In the Patient 1 scar_25% scenario (Fig. 4 B), the area under the graphs decreased compared to the no scar scenario since there was less healthy LV-volume that could be recruited, as seen in Supplementary

Video 2. The same trend was observed in terms of posterior sites producing the highest MAF, but with a greater correlation between MAF and activation delay (the time it took the activation of the RV to reach the site), r = 0.905, n = 11, p = 0.000. The scar caused the final part of the activation front graph to stretch over a longer time since the activation front must propagate *around* the scar, resulting in higher TAT values. The upstroke of the apical and anterior sites followed a similar path to the no-scar scenario initially until the activation front reached the scar (see Supplementary Video 2) and the curve started to plateau. This is reflected in low MAF values. Five out of twelve sites in this model produced lower MAF than baseline. The apical site produced the lowest MAF, 23 % lower than the baseline. Upstroke from posterior site pacing was slower than in the scenario without scar since scar in the posterior region of the LV had an immediate effect on the activation front. The result of mid.p site is identical to the baseline since it lies within the scar (see Fig. 2). The mid.p-l site produced the highest MAF, 36 % higher than baseline. As seen in Supplementary Video 2 (best SSP) the scar decelerated the activation front of mid.p-l, and MAF was reached when reaching the RV-site midway trajectory.

3.1.1 Changing scar size

An overview of the MAF values in SSP is displayed in bullseye representation in Fig. 5, where the color of each segment indicates the MAF value when that segment was paced. It shows that in Patient 1, changing scar size did not affect results much, with apical and anterior pacing producing the lowest- and posterior sites the highest MAF values. The smallest scars (1.5% and 5%) produced recruitment curves similar to the no-scar scenario, while in scar_10%, the effect is more evident and resembling the results seen in scar_25% with mid.p being active and not in the scar. The larger the scar, the lower the MAF became and the graph of the worse configurations became flatter, especially when apical sites were involved.

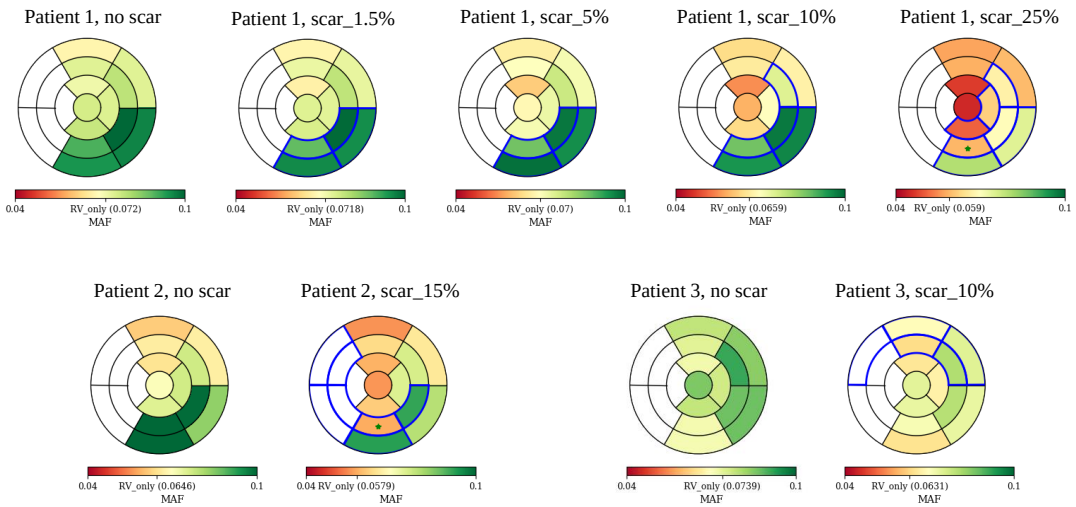

Figure 5 Bullseye representation of MAF values for SSP of all the scenarios. The color of each segment represents the resulting MAF value when pacing from that segment. The segments containing scar tissue are outlined in blue. The star indicates segments with complete scar.

3.1.2 Changing scar location

In Patient 2 and Patient 3 with no scar, similar to Patient 1, the anterior and apical sites produced the lowest MAF values, while the highest was produced by the posterior sites in Patient 2 and the lateral sites in Patient 3. In the scar scenarios, a similar trend as in Patient 1 was observed for Patient 2, but in Patient 3 there was no clear favorable pacing location, with mid.a-l site producing the highest MAF and mid.a producing the lowest. The MAF difference was only 0.017 between the highest and lowest MAF in Patient 3 compared to 0.035 and 0.037 in Patient 1 and Patient 2, respectively.

3.2 Multisite pacing

In-Patient 1, pacing the LV from two sites (DSP) produced sharper upstroke and shorter TAT compared to pacing from a single LV site, but MAF values did not always increase. In the no-scar scenario, from 66 different DSP configurations, only 20 produced higher MAF than the MAF produced by the best SSP site. As seen in Fig. 6 A, which shows the best and worst DSP results, the MAF had a range of 0.067 (0.132 – 0.065) compared to the range of 0.031 (0.1 - 0.069) of the SSP. This indicates that in DSP, the positioning of pacing sites has a greater effect on MAF values. The highest MAF of 0.132 was produced by pacing mid.p and mid.a-l, 32 % higher than the best SSP. As seen in Fig. 6 A, some DSP configurations produced similar MAF values (mid.p&api.l and bas.p&mid.a-l), but with completely different site configurations. The lowest MAF values were produced by adjacent site pairs, with the combination of two anterior or two apical sites being the worst (See the top three in the legend of Fig. 6 A). The activation fronts of these adjacent site pairs produce steeper upstroke than SSP from the same locations (see Apical sites in Fig. 4 A). When the activation fronts merge, the specific LV region is then activated even faster and the graph plateaus earlier, producing MAF values even lower than the worse SSP in some cases.

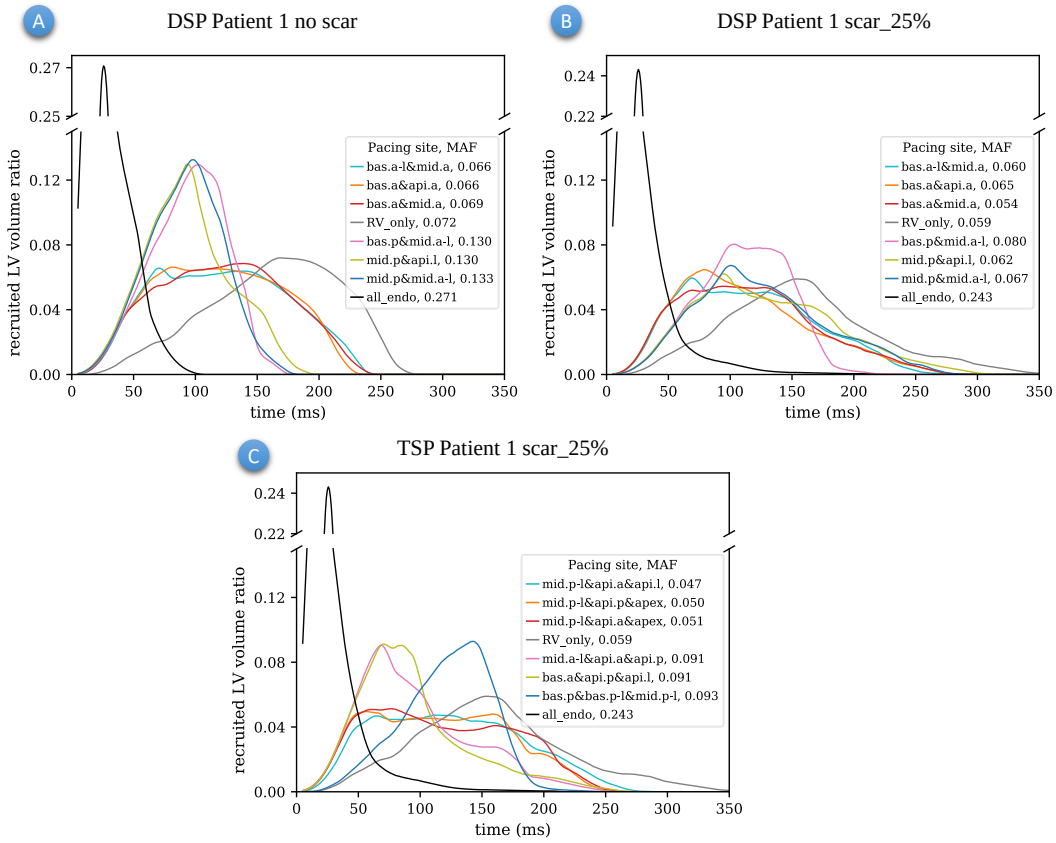

Figure 6 LV activation front graphs of the DSP and TSP . A (no scar) and B (scar) show the results of best and worst DSP configurations, along with RV_only and all_endo. C shows the three best and three worst TSP configurations. The results involving site mid.p were excluded from the scar_25% results as it lied within the scar.

In the scenario with scar_25%, only 5 DSP configurations produced higher MAF than the best SSP, produced by bas.p. All 5 included bas.p and a lateral site (Fig. 6 B). The lowest MAF values were produced by pacing two adjacent sites including at least one apical site. Such combinations had superior upstroke as their activation fronts merge with the one from the RV-site early, and once the combined front reaches the scar it propagates around it and the curve plateaus. In configurations with higher MAF values, the LV pacing-sites are in the sites with the longest activation delay (See Table 1) and their activation fronts do not merge before activating large areas around the scar. This produces slower upstroke, but a larger area around the scar is activated within a shorter period, lowering TAT, resulting in higher MAF and more synchrony.

Adding a third LV site (TSP) did improve outcomes, but only slightly, with the average MAF of all TSP configurations being 0.071 compared to 0.065 of DSP. The best and worst values, however, are comparable. Also, in TSP, a combination of apical sites produce the lowest MAF values. Site mid.p-l appeared in the worst configurations both in DSP and TSP due to the location within the grey zone. The highest MAF with TSP was achieved by combining mid.p-l with the best DSP pair, which produced a similar graph to the best DSP configuration. The next-best TSP-combination produced similar MAF values but much steeper upstroke (see Fig. 6 C). These included combinations of apical and anterior sites surrounding the scar.

3.2.1 Changing scar size

Fig. 7 shows the recruitment graphs of Patient 1 with smaller scars. Like in the no scar scenario, with scar_1.5%, 20 of the 66 DSP configurations (30 %) produced higher MAF than the best SSP, while in scar_5% and scar_10%, it was achieved by 18 (27 %) and 14 (21 %) DSP configurations, respectively. As mentioned earlier, with scar_25% only 5 (9 %) DSP configurations improved MAF compared to the best SSP. The big difference between scar_25% and the smaller scars may not only be due to scar size but also that the site mid.p was favorable in smaller scars where this site did not lie within the non-conductive scar.

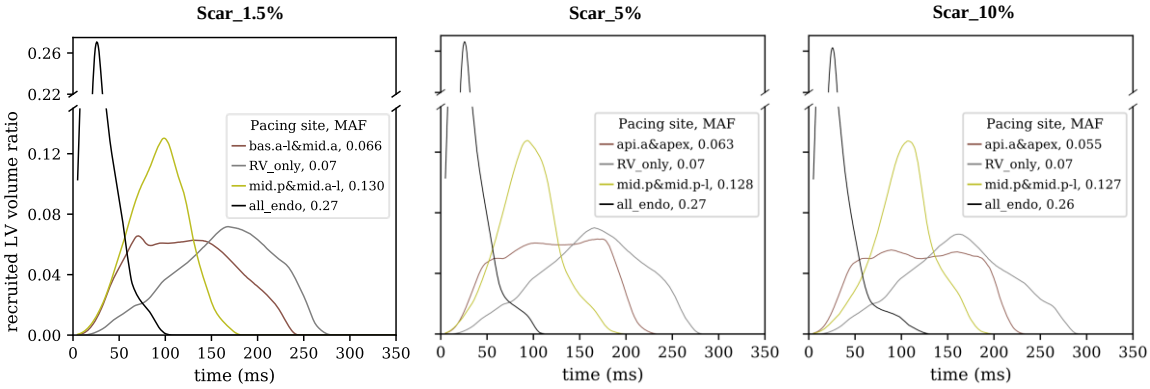

Figure 7 LV activation front graphs of the best and worst DSP configuration of the different scar sizes of Patient 1.

3.2.2 Changing Scar Location

In the scar scenarios, DSP had a greater effect in Patient 3, with the best DSP producing 42 % higher MAF than the best SSP, compared to the 1.5 % and 4.5 % increase in Patients 1 (scar_25%) and Patient 2. Consistently in all three patients, DSP from two apical sites produced the worst outcome. As seen in Fig. 8, similar high MAF values are achieved by multiple DSP configurations. In Patient 2, who has a posteroseptal scar, bas.a and mid.p-l produced the highest MAF, whereas mid.a-l and api.p produced the highest MAF in Patient 3 who has an anterior scar. Some combinations that included a posterior or a lateral site produced inferior outcomes. These facts highlight the need for a tool to help evaluate various pacing configurations carefully. Table 3 shows a summary of all the results.

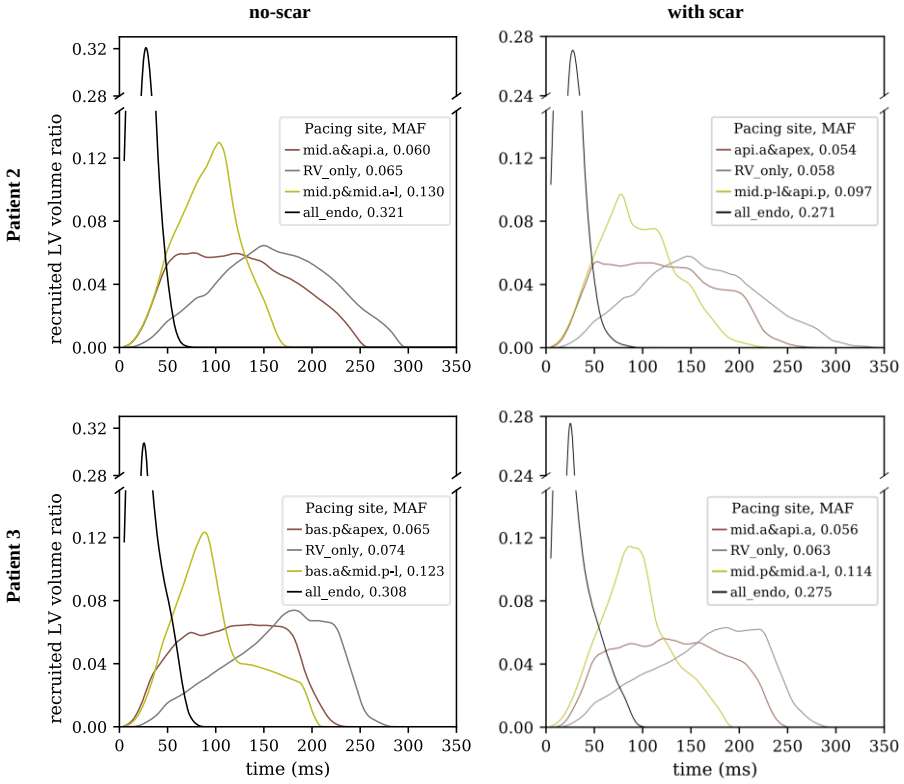

Figure 8 LV activation front graphs of the best and worst DSP configuration of Patient 2 and Patient 3.

3.3 Conventional pacing and MAF

The highest MAF value of the DSP is considered the theoretical maximum MAF (MAFmax). To illustrate how conventional CRT pacing ranks compared to MAFmax, we introduce ΔMAF, the percentage of a MAF from the MAFmax (Table 2). Conventional CRT, referred to as clinical SSP, representing clinically standard CRT, is assumed to be when pacing the LV from the middle posterolateral site, which is the target site according to AHA guidelines [(34)]. When DSP is used clinically it is assumed to be optimal when pacing from the basal anterior site is added representing the site furthest away from both the RV site and the posterolateral site. This has been the most common approach in MSP studies [(35)]. As seen in Table 2, optimal SSP in all our simulations provides similar or only slightly higher ΔMAF compared to what is expected from clinical SSP. Adding a second LV site in the most distant site (clinical DSP) did not produce the best results and in the Patient 1 scar_25% scenario it even produced lower ΔMAF.

Patient	Scenario	**Clinical SSP**	**Optimal SSP**		**Clinical DSP**	**Optimal DSP (MAFmax)**	
		ΔMAF	sites	ΔMAF	ΔMAF	sites	MAF
1	scar_0%	76%	mid.p-l	76%	84%	mid.p&mid.a-l	0.132
	scar_25%	75%	bas.p	87%	65%	bas.p&bas.p-l	0.921
2	scar_0%	76%	mid.p	77%	77%	mid.p&mid.a-l	0.130
	scar_15%	95%	bas.p	96%	99%	mid.p-l&api.p	0.097
3	scar_0%	70%	mid.a-l	74%	100%	bas.a&mid.p-l	0.123
	scar_10%	76%	mid.a-l	80%	93%	mid.p&mid.a-l	0.114

Table 2 Clinical versus theoretically optimal pacing configurations. Clinical SSP: mid.p-l, Clinical DSP: mid.p-l&bas.a, MAFmax: maximum achievable MAF with DSP, ΔMAF: MAF/MAFmax.

		Patient 1										Patient 2				Patient 3			
		No scar		**Scar_1.5%**		**Scar_5%**		**Scar_10%**		**Scar_25%**		**No scar**		**Scar_15%**		**No scar**		**Scar_10%**	
Baseline MAF		0.072		0.072		0.07		0.066		0.059		0.065		0.058		0.074		0.063	
All endo (best-case)		0.271		0.271		0.269		0.263		0.243		0.321		0.271		0.308		0.275	
		Sites	MAF	Sites	MAF	Sites	MAF	Sites	MAF	Sites	MAF	Sites	MAF	Sites	MAF	Sites	MAF	Sites	MAF
SSP	Best	11	0.100	11	0.100	4	0.099	11	0.098	4	0.080	10	0.100	4	0.093	12	0.091	12	0.081
	Worst	1	0.069	13	0.067	13	0.061	13	0.055	17	0.045	1	0.062	1	0.056	10	0.072	7	0.064
	avg		**0.082**		**0.080**		**0.078**		**0.075**		**0.065**		**0.078**		**0.069***		**0.079**		**0.071**
DSP	Best	10-12	0.132	10-12	0.131	10-11	0.128	10-11	0.128	4-5	0.092	10-12	0.130	11-15	0.097	1-11	0.123	10-12	0.114
	Worst	6-7	0.065	6-7	0.065	13-17	0.062	13-17	0.055	13-16	0.047	7-13	0.060	13-17	0.054	4-17	0.065	7-13	0.056
	avg		**0.093**		**0.091**		**0.090**		**0.083**		**0.065***		**0.086**		**0.078***		**0.090**		**0.081**
TSP	Best									4-5-11	0.093								
	Worst									11-13-16	0.047								
	avg										**0.071***								

*Table 3 Summary of the results. Sites numbers refer to the segment numbers the sites are in (see Table 1). The baseline refers to RV-only pacing and all sites are when all the sites are paced simultaneously representing a theoretical best-case scenario. SSP: Single-site pacing, DSP: Dual-site pacing, TSP: Triple-site pacing. avg: the average MAF of all the respective configurations. *: Site 10 (mid.p) is excluded as it lies within the scar.*

4 Discussion and Conclusion

4.1 Discussion

Determining the optimal LV pacing site remains an important challenge in CRT. Suboptimal LV pacing sites may contribute to high non-response rates. Responders are clinically identified based on improved symptoms and echocardiographic evidence of improved cardiac function. Reverse remodeling occurring following implantation is commonly assessed 3 to 6 months after CRT. Peri-operative measurements, such as maximum LV pressure gradient (dP/dt_{max}) or TAT measures, have not shown a consistent relationship to long-term response [8, 9]. Studying alternative outcome measurements for prediction and alternative pacing approaches is therefore important.

In this study, we used computational modeling to analyze the electrical activation front. Based on these investigations we propose the use of MAF as an outcome parameter for optimization of pacing configuration. When pacing the LV, the stimulus propagates throughout the myocardium, recruiting cardiomyocytes sequentially, until the whole LV is recruited within the TAT. Reducing TAT is reportedly associated with better outcomes, but TAT by itself is not an indicator of synchrony and is not a satisfactory measure of CRT outcome [36]. A prolonged TAT may result from a small fraction of the LV not important for overall function, is activated late. There may be conduction delay in a larger part of the LV without influence on TAT but without improving synchrony. This is reflected by reduced MAF and preserved TAT, demonstrated by slow upstroke of the recruitment curve. Although MAF seems to be superior, a measure that combines TAT and MAF might be even better than MAF alone. MAF may be sensitive to the thickness of the LV section being paced, while TAT is not (see 3.1).

Electrical activation fronts are decelerated when reaching boundaries of fibrotic or refractory tissue, slowing or halting propagation in one or more directions. The overall boundaries are represented by the anatomical limitations of the heart. When multiple stimuli are considered, the highest MAF is reached when all activation fronts merge at the latest possible time. This is shown in the results of SSP where, in all three patients, pacing from the sites with the longest activation delay produced the best MAF. This is in keeping with long-term results seen when pacing from sites with a larger electrical separation [37]. Pacing the latest activated area with SSP is recommended by large clinical studies and are associated with long-term improvements [38, 39]. This finding supports our suggestion of using MAF as an alternative predictor. Fig. 5 shows how the MAF values of the different sites change with different scar sizes and locations. In the largest scars, outcomes from the worst sites become even worse and optimal sites become more evident. Although the optimal SSP site is located intuitively in the latest activated area, it is not always accessible through the coronary sinus. Defining the best accessible sites (next-best) is more complex and requires careful assessment of venous anatomy as it relates to the recommended pacing sites, and results from SSP may be improved by more versatile anatomic placement-modalities for electrodes.

Certain pacing configurations produced similar MAF values, but with different upstrokes in the recruitment curve. A slightly lower MAF value may be an acceptable trade-off for a steeper upstroke, but a steeper upstroke with unchanged MAF is associated with longer TAT. Fig. 6 C shows that the graph with the next-highest MAF value (bas.a&api.p&api.l) has a steeper upstroke, but after the maximum (MAF) the curve decays at a slower pace, producing longer TAT. This characteristic is discussed by Periera et al. [40], who argue that *time of bulk activation*, which is the time between 10 % and 90 % of the ventricular volume is activated, maybe a more relevant predictor of CRT response than TAT. Steepening the upstroke of the recruitment curves without increasing MAF, will only increase the time of bulk activation. Our SSP results are in line with this study and with clinical observations of conventional CRT.

Multisite pacing (MSP) aims to improve CRT outcomes by pacing the LV from two or more sites [41]. Several studies demonstrated improved acute and long-term outcomes of MSP compared to conventional single-site pacing (SSP), while others showed similar outcomes [42]. Patients with sizable myocardial scars are less likely to respond to CRT compared to patients without- or with- small scars [43] and electrode placement is more important in the presence of scars [44, 45]. The concept of MSP is relatively new, and the effect of pacing sites is not fully understood. MSP studies commonly place the second LV electrode as distant as possible from the other LV and the RV sites [46-49]. Our study indicates that MAF measurements may provide insight into and improve outcomes of MSP and other pacing configurations.

A theoretical, optimal pacing configuration based on maximum achievable MAFmax, may serve as a valuable benchmark. A typical clinical configuration with one RV and one LV electrode placed in the apex and lateral wall distant apart created a MAF that was expressed as a fraction in percent of MAFmax. This percentage can be viewed as a target. Adding an electrode (Conventional DSP) does not always improve the outcome and could even make it worse (see Table 2). By repositioning electrodes higher values may be obtained suggesting better resynchronization. We believe that may take place, demonstrating that MAF/MAFmax may serve as a clinical parameter for the optimization of pacing configurations.

When an additional LV site is included, activation fronts become more complex. DSP improved MAF, but only when sites are optimally situated. Maximum MAF occurred when the combination of sites was located electrically remotely from the RV-site, from the base, and each other. How to combine sites that should be electrically remote from each other and least affected by scars is often not easily accomplished. Our study shows that if sites are not properly chosen, outcomes of MSP may not be improved or even worsen compared to optimally selected SSP sites. Jackson et al. [48], showed no significant benefit of DSP compared to optimized SSP. In their report, SSP was chosen carefully, while in DSP the additional lead was placed as far as possible from the first lead without other considerations. Our results indicate that a more complicated determination of the relationship between sites is required

to achieve optimal outcomes. Computational modeling may at present be the best way to define optimal, non-intuitive combinations of electrode placements. Adding a third LV pacing site did not increase MAF notably, but increased the chance of achieving optimal DSP configuration and could produce MAF values up to 30 % higher than SSP. Considering the potential clinical challenges and possible complications, inserting a third LV lead may not be practical, but with a quadripolar lead or surgical lead placement, MSP may be achievable.

4.2 Study Limitations

The main benefit of in silico models is the ability to help us understand complex processes and to study the effect of different factors separately. This approach requires assumptions and simplifications that may influence results compared to the clinical situation. In this study, we used the individual patient's heart geometry as an input to the model, while keeping fiber orientation and conduction velocities generic. The Purkinje network, which, when present may affect pacing outcomes, was also assumed to be absent in our simulations.

The main indication for CRT is left bundle branch block and prolonged QRS complex in HF patients. Electro-mechanically coupled computational models for investigation of various pacing strategies may be useful in the planning of CRT, but such models are currently relatively coarse due to high complexity and requirements for computational power. Since mechanical activation is governed by the electrical stimulation of the cardiomyocytes, the assumption that optimizing electrical activation will lead to improved mechanical performance seems reasonable. The rapid access to artificial intelligence and increased computing power may make advanced simulations, including the addition of mechanical parameters more reliable and faster.

The patients included in this study were patients with ischemic heart disease and normal conduction without typical indications for CRT. However, such patients frequently become candidates for pacemaker therapy, and CRT is a therapeutic option in patients with ischemic heart disease and depressed LV-function who has an indication for pacing. The patients were initially recruited for a computational modeling study to predict arrhythmia in ischemic heart disease [(23)]. We believe these patients served well for the purpose and validation of our model as they had complex geometries with ischemic regions. For the upcoming prospective clinical study, candidates with classic indications for CRT will be recruited.

4.3 Conclusion

We use an electrophysiological computational model, including patient scenarios with myocardial scars, to analyze various pacing configurations using the novel parameter MAF. In line with clinical observations, the best outcomes in SSP are achieved when pacing the latest activated area independent of scar size or location, given that the pacing site is not located within the scar itself. Finding the optimal MSP using two different LV pacing sites is a complex task and associated with the electrical pathways

between pacing sites, RV, the base of the heart, and scar(s). In our opinion, MAF appears to be a good measure that incorporates synchrony and activation time in one parameter. Further computational and clinical studies are required to fully understand the underlying mechanisms of CRT effectiveness and the potential of MAF as a global CRT outcome predictor.

Acknowledgment

This work was funded by the European Union's H2020: MSCA: ITN program for the "Wireless In-body Environment Communication – WiBEC" project under the grant agreement no. 675353.

References

1. Savarese G, Lund LH. Global public health burden of heart failure. Cardiac failure review. 2017;3(1):7.
2. Members ATF, Brignole M, Auricchio A, Baron-Esquivias G, Bordachar P, Boriani G, et al. 2013 ESC Guidelines on cardiac pacing and cardiac resynchronization therapy: the Task Force on cardiac pacing and resynchronization therapy of the European Society of Cardiology (ESC). Developed in collaboration with the European Heart Rhythm Association (EHRA). European heart journal. 2013;34(29):2281-329.
3. Cleland JG, Daubert J-C, Erdmann E, Freemantle N, Gras D, Kappenberger L, et al. The effect of cardiac resynchronization on morbidity and mortality in heart failure. New England Journal of Medicine. 2005;352(15):1539-49.
4. Auricchio A, Stellbrink C, Sack S, Block M, ürgen Vogt J, Bakker P, et al. Long-term clinical effect of hemodynamically optimized cardiac resynchronization therapy in patients with heart failure and ventricular conduction delay. Journal of the American College of Cardiology. 2002;39(12):2026-33.
5. Abraham WT, Fisher WG, Smith AL, Delurgio DB, Leon AR, Loh E, et al. Cardiac resynchronization in chronic heart failure. New England Journal of Medicine. 2002;346(24):1845-53.
6. Albatat M, Bergsland J, Arevalo H, Odland HH, Bose P, Halvorsen PS, et al. Technological and clinical challenges in lead placement for cardiac rhythm management devices. Annals of Biomedical Engineering. 2020;48(1):26-46.
7. Singh JP, Berger RD, Doshi RN, Lloyd M, Moore D, Stone J, et al. Targeted Left Ventricular Lead Implantation Strategy for Non-Left Bundle Branch Block Patients: The ENHANCE CRT Study. 2020.
8. Saxon LA, Olshansky B, Volosin K, Steinberg JS, Lee BK, Tomassoni G, et al. Influence of left ventricular lead location on outcomes in the COMPANION study. Journal of cardiovascular electrophysiology. 2009;20(7):764-8.
9. Singh JP, Klein HU, Huang DT, Reek S, Kuniss M, Quesada A, et al. Left Ventricular Lead Position and Clinical Outcome in the Multicenter Automatic Defibrillator Implantation Trial–Cardiac Resynchronization Therapy (MADIT-CRT) Trial. Circulation. 2011;123(11):1159-66.
10. Ruschitzka F, Abraham WT, Singh JP, Bax JJ, Borer JS, Brugada J, et al. Cardiac-resynchronization therapy in heart failure with a narrow QRS complex. N Engl J Med. 2013;369(15):1395-405.
11. Lee AWC, Costa CM, Strocchi M, Rinaldi CA, Niederer SA. Computational Modeling for Cardiac Resynchronization Therapy. J Cardiovasc Transl Res. 2018;11(2):92-108.
12. Huntjens PR, Walmsley J, Ploux S, Bordachar P, Prinzen FW, Delhaas T, et al. Influence of left ventricular lead position relative to scar location on response to cardiac resynchronization therapy: a model study. Europace. 2014;16(suppl_4):iv62-iv8.
13. Niederer SA, Shetty A, Plank G, Bostock J, Razavi R, Smith N, et al. Biophysical modeling to simulate the response to multisite left ventricular stimulation using a quadripolar pacing lead. Pacing and Clinical Electrophysiology. 2012;35(2):204-14.
14. Kerckhoffs RC, McCulloch AD, Omens JH, Mulligan LJ. Effects of biventricular pacing and scar size in a computational model of the failing heart with left bundle branch block. Medical image analysis. 2009;13(2):362-9.

15. Sermesant M, Chabiniok R, Chinchapatnam P, Mansi T, Billet F, Moireau P, et al. Patient-specific electromechanical models of the heart for the prediction of pacing acute effects in CRT: a preliminary clinical validation. Medical image analysis. 2012;16(1):201-15.

16. Constantino J, Hu Y, Trayanova NA. A computational approach to understanding the cardiac electromechanical activation sequence in the normal and failing heart, with translation to the clinical practice of CRT. Progress in biophysics and molecular biology. 2012;110(2):372-9.

17. Hu Y, Gurev V, Constantino J, Trayanova N. Optimizing cardiac resynchronization therapy to minimize ATP consumption heterogeneity throughout the left ventricle: a simulation analysis using a canine heart failure model. Heart Rhythm. 2014;11(6):1063-9.

18. Villongco CT, Krummen DE, Omens JH, McCulloch AD. Non-invasive, model-based measures of ventricular electrical dyssynchrony for predicting CRT outcomes. EP Europace. 2016;18(suppl_4):iv104-iv12.

19. Marciniak M, Arevalo H, Tfelt-Hansen J, Jespersen T, Jabbari R, Glinge C, et al., editors. From CMR image to patient-specific simulation and population-based analysis: tutorial for an openly available image-processing pipeline. International Workshop on Statistical Atlases and Computational Models of the Heart; 2016: Springer.

20. Schroeder WJ, Lorensen B, Martin K. The visualization toolkit: an object-oriented approach to 3D graphics: Kitware; 2004.

21. Geuzaine C, Remacle JF. Gmsh: A 3-D finite element mesh generator with built-in pre-and post-processing facilities. International journal for numerical methods in engineering. 2009;79(11):1309-31.

22. Bayer J, Blake R, Plank G, Trayanova N. A novel rule-based algorithm for assigning myocardial fiber orientation to computational heart models. Annals of biomedical engineering. 2012;40(10):2243-54.

23. Jabbari R, Engstrøm T, Glinge C, Risgaard B, Jabbari J, Winkel BG, et al. Incidence and risk factors of ventricular fibrillation before primary angioplasty in patients with first ST-elevation myocardial infarction: a nationwide study in Denmark. 2015;4(1):e001399.

24. Ten Tusscher K, Noble D, Noble P, Panfilov A. A model for human ventricular tissue. American Journal of Physiology-Heart and Circulatory Physiology. 2004;286(4):H1573-H89.

25. Clayton RH, Panfilov AV. A guide to modelling cardiac electrical activity in anatomically detailed ventricles. Prog Biophys Mol Biol. 2008;96(1-3):19-43.

26. Hooks DA, Trew ML, Caldwell BJ, Sands GB, LeGrice IJ, Smaill BH. Laminar arrangement of ventricular myocytes influences electrical behavior of the heart. Circ Res. 2007;101(10):e103-12.

27. Pu J, Boyden PA. Alterations of Na+ currents in myocytes from epicardial border zone of the infarcted heart. A possible ionic mechanism for reduced excitability and postrepolarization refractoriness. Circ Res. 1997;81(1):110-9.

28. Dun W, Baba S, Yagi T, Boyden PA. Dynamic remodeling of K+ and Ca2+ currents in cells that survived in the epicardial border zone of canine healed infarcted heart. Am J Physiol Heart Circ Physiol. 2004;287(3):H1046-54.

29. Jiang M, Cabo C, Yao J, Boyden PA, Tseng G. Delayed rectifier K currents have reduced amplitudes and altered kinetics in myocytes from infarcted canine ventricle. Cardiovasc Res. 2000;48(1):34-43.

30. Yao JA, Hussain W, Patel P, Peters NS, Boyden PA, Wit AL. Remodeling of gap junctional channel function in epicardial border zone of healing canine infarcts. Circ Res. 2003;92(4):437-43.

31. Vigmond EJ, Hughes M, Plank G, Leon LJ. Computational tools for modeling electrical activity in cardiac tissue. J Electrocardiol. 2003;36 Suppl:69-74.

32. Vigmond EJ, Weber dos Santos R, Prassl AJ, Deo M, Plank G. Solvers for the cardiac bidomain equations. Prog Biophys Mol Biol. 2008;96(1-3):3-18.

33. Cerqueira MD, Weissman NJ, Dilsizian V, Jacobs AK, Kaul S, Laskey WK, et al. Standardized myocardial segmentation and nomenclature for tomographic imaging of the heart. A statement for healthcare professionals from the Cardiac Imaging Committee of the Council on Clinical Cardiology of the American Heart Association. Circulation. 2002;105(4):539-42.

34. Yancy CW, Jessup M, Bozkurt B, Butler J, Casey DE, Drazner MH, et al. 2013 ACCF/AHA guideline for the management of heart failure: a report of the American College of Cardiology Foundation/American Heart Association Task Force on Practice Guidelines. Journal of the American College of Cardiology. 2013;62(16):e147-e239.

35. Albatat M, Bergsland J, Arevalo H, Odland HH, Wall S, Sundnes J, et al. Multisite pacing and myocardial scars: a computational study. Computer Methods in Biomechanics and Biomedical Engineering. 2020:1-13.

36. Yu C, Lin H, Zhang Q, Sanderson J. High prevalence of left ventricular systolic and diastolic asynchrony in patients with congestive heart failure and normal QRS duration. Heart. 2003;89(1):54-60.

37. Field ME, Yu N, Wold N, Gold MRJHr. Comparison of measures of ventricular delay on cardiac resynchronization therapy response. 2020;17(4):615-20.

38. Ypenburg C, van Bommel RJ, Delgado V, Mollema SA, Bleeker GB, Boersma E, et al. Optimal left ventricular lead position predicts reverse remodeling and survival after cardiac resynchronization therapy. Journal of the American College of Cardiology. 2008;52(17):1402-9.

39. Khan FZ, Virdee MS, Palmer CR, Pugh PJ, O'Halloran D, Elsik M, et al. Targeted left ventricular lead placement to guide cardiac resynchronization therapy: the TARGET study: a randomized, controlled trial. Journal of the American College of Cardiology. 2012;59(17):1509-18.

40. Pereira H, Jackson TA, Claridge S, Yao C, Sieniewicz B, Gould J, et al. Evidence of reverse electrical remodelling by non-invasive electrocardiographic imaging to assess acute and chronic changes in bulk ventricular activation following cardiac resynchronisation therapy. Journal of Electrocardiology. 2020;58:96-102.

41. Pappone C, Rosanio S, Oreto G, Tocchi M, Gulletta S, Salvati A, et al. Cardiac pacing in heart failure patients with left bundle branch block: impact of pacing site for optimizing left ventricular resynchronization. Italian heart journal: official journal of the Italian Federation of Cardiology. 2000;1(7):464-9.

42. Antoniadis AP, Sieniewicz B, Gould J, Porter B, Webb J, Claridge S, et al. Updates in Cardiac Resynchronization Therapy for Chronic Heart Failure: Review of Multisite Pacing. Current heart failure reports. 2017;14(5):376-83.

43. Mangiavacchi M, Gasparini M, Faletra F, Klersy C, Morenghi E, Galimberti P, et al. Clinical predictors of marked improvement in left ventricular performance after cardiac resynchronization therapy in patients with chronic heart failure. Am Heart J. 2006;151(2):477 e1- e6.

44. Rademakers LM, van Kerckhoven R, van Deursen CJ, Strik M, van Hunnik A, Kuiper M, et al. Myocardial infarction does not preclude electrical and hemodynamic benefits of cardiac resynchronization therapy in dyssynchronous canine hearts. Circ Arrhythm Electrophysiol. 2010;3(4):361-8.

45. Delgado V, van Bommel RJ, Bertini M, Borleffs CJW, Marsan NA, Ng AC, et al. Relative Merits of Left Ventricular Dyssynchrony, Left Ventricular Lead Position, and Myocardial Scar to Predict Long-Term Survival of Ischemic Heart Failure Patients Undergoing Cardiac Resynchronization TherapyClinical Perspective. Circulation. 2011;123(1):70-8.

46. Ginks MR, Shetty AK, Lambiase PD, Duckett SG, Bostock J, Peacock JL, et al. Benefits of Endocardial and Multisite Pacing Are Dependent on the Type of Left Ventricular Electric Activation Pattern and Presence of Ischemic Heart Disease Insights from Electroanatomic Mapping. Circulation: Arrhythmia and Electrophysiology. 2012;5(5):889-97.

47. Rinaldi CA, Kranig W, Leclercq C, Kacet S, Betts T, Bordachar P, et al. Acute effects of multisite left ventricular pacing on mechanical dyssynchrony in patients receiving cardiac resynchronization therapy. Journal of cardiac failure. 2013;19(11):731-8.

48. Jackson T, Lenarczyk R, Sterlinski M, Sokal A, Francis D, Whinnett Z, et al. Left ventricular scar and the acute hemodynamic effects of multivein and multipolar pacing in cardiac resynchronization. IJC Heart & Vasculature. 2018;19:14-9.

49. Leclercq C, Gadler F, Kranig W, Ellery S, Gras D, Lazarus A, et al. A randomized comparison of triple-site versus dual-site ventricular stimulation in patients with congestive heart failure. Journal of the American College of Cardiology. 2008;51(15):1455-62.